Nano-displacement sensor based on photonic crystal fiber modal interferometer

Jitendra Narayan Dash,[1] Rajan Jha,[1,*] Joel Villatoro,[2,3] and Sumit Dass[1]

[1]*Nanophotonics and Plasmonics Laboratory, School of Basic Sciences, IIT Bhubaneswar, Toshali Bhawan, India*

[2]*Department of Communications Engineering, Escuela Técnica Superior de Ingeniería (ETSI) de Bilbao, University of the Basque Country (UPV/EHU), Alda. Urquijo s/n, E-48013 Bilbao, Spain*

[3]*IKERBASQUE, Basque Foundation for Science, E-48011 Bilbao, Spain*

**Corresponding author: rajaniitd@gmail.com*

Received November 17, 2014; revised December 26, 2014; accepted December 28, 2014; posted January 7, 2015 (Doc. ID 226901); published February 4, 2015

A stable nano-displacement sensor based on large mode area photonic crystal fiber (PCF) modal interferometer is presented. The compact setup requires simple splicing of a small piece of PCF with a single mode fiber (SMF). The excitation and recombination of modes is carried out in a single splice. The use of a reflecting target creates an extra cavity that discretizes the interference pattern of the mode interferometer, boosting the displacement resolution to nanometer level. The proposed modal interferometric based displacement sensor is highly stable and shows sensitivity of 32 pm/nm. © 2015 Optical Society of America

OCIS codes: (060.2370) Fiber optics sensors; (060.5295) Photonic crystal fibers; (120.3180) Interferometry; (280.4788) Optical sensing and sensors.

http://dx.doi.org/10.1364/OL.40.000467

Displacement sensors have much significance in various scientific and technological applications as they can be used for precision alignment or position monitoring. Thus, displacement sensors have applications in fields such as medical sector, structural health monitoring, and aeronautics [1–3]. For such applications, it is important to measure displacements in the submicron scale accurately with a sensor as simple as possible. Various types of displacement sensors based on electronic and fiber optic techniques have been reported [4,5]. However, because of the advantages like electromagnetic immunity, miniature size, low weight, and remote sensing capability, the fiber optic based sensors have an edge over electronic based sensors [6]. Riding on the advantages of fiber based sensors, several displacement sensors like Fabry–Perot interferometric sensor, white light fiber optic interferometer, fiber Bragg grating, and long period fiber gratings have been reported [7–10]. In the case of white light fiber optic interferometer, the position measurement has been reported with 6 nm resolution over a 100 μm range [8]. However, to detect the position, an algorithm based on the fitting of an auto correlation function of the captured optical power spectrum has to be used which may compromise the accurate determination of the displacement. The use of fiber Bragg grating based sensors for displacement measurement suffers from design fabrication complexities and has a sensitivity of 37.9 mv/mm which is in millimeter range. A micro Fabry–Perot sensor for nano lateral displacement has been demonstrated [11]. However, the device uses liquids and flexible membrane leading to the change in cavity parameter because of high stress. In addition to the above sensors, subnanometer displacement sensors based on laser heterodyne interferometry have been reported [12,13]. However, the setup uses several optical components and the oscillation frequency of the laser has to be stabilized.

To make the sensor design compact and easier for fabrication, photonic crystal fibers (PCFs) based on modified total internal reflection guidance and band gap guidance have been used for designing displacement sensors [14–18]. The superior modal and guidance properties make PCF better than the conventional fibers [19]. Transverse displacement sensors have been reported using the birefringent nature of PCF coils [14]. Here stress has to be applied on the PCF which limits its application. Moreover, the displacement sensing sensitivity of the PCF coil is 90.4 nm/mm. In addition, Sagnac loop sensors based on Hi–Bi fiber with low sensitivity (0.28286 nm/mm) have been reported [16]. However, in this case, two splicing joints are required which may affect the stability of the sensor. The hollow-core PCF based micro displacement sensor reported in [17] has some drawbacks. The SMF-hollow-core PCF junction is fragile; the device can only be operated over a narrow wavelength range. In addition, the resolution of the device is in micrometer range and the measuring range is only a few micrometers [17]. Displacement sensing based on a photonic crystal waveguide using numerical simulation has also been suggested, but not demonstrated [18].

In this Letter, we report on an interferometric nano-displacement sensor based on solid core PCF. The proposed sensor is robust and easy to fabricate as it requires cleaving and fusion splicing [20]. In this design, only one end of the PCF is used for splicing and the other end remains open as shown in Fig. 1. As a target, we used a mirror that was displaced in nanometer steps with the help of a high-precision computer-controlled positioner from Piezosystem, Jena for calibration. The interference pattern of our device is coupled to that formed by the end face of the PCF and the target. This discretizes the broad interference pattern of the mode interferometer and improves the detection resolution.

The detailed schematic diagram of the experimental setup is shown in Fig. 1. The light from the superluminescent light emitting diode (SLED) is launched to the circulator which, in turn, couples the light to the sensor head consisting of an SMF spliced to the PCF. A part of

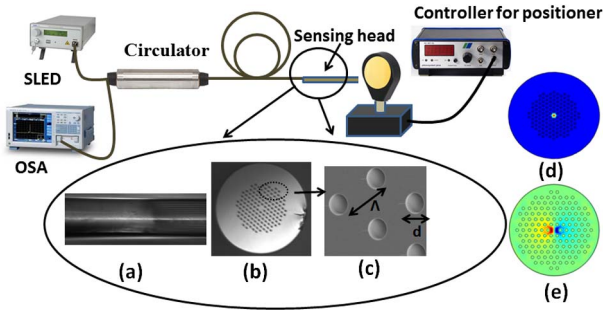

Fig. 1. Schematic diagram of experimental setup for displacement sensing. The inset (a) shows the splicing joint of SMF and PCF, (b) shows the cross section of the PCF, (c) shows the zoomed view of a section of PCF with $d = 2.32$ μm and pitch $\Lambda = 5.6$ μm, and (d)–(e) show the fundamental and LP_{11} mode of the PCF, respectively. SLED refers to super luminescent light emitting diode, and OSA refers to optical spectrum analyzer.

the light reflected from the PCF facet is again coupled back to the circulator and is collected in another port for analysis through OSA (Yokogawa AQ 6319). The PCF used in the experiments had a core diameter of 8.5 μm and a diameter of 125 μm with a mode field diameter of 7 ± 1 μm. The core is surrounded by seven rings of air holes arranged in a triangular lattice, as seen in Fig. 1(b). The average diameter of the air holes is 2.32 μm, while the pitch of the air holes is 5.6 μm. The filling factor (d/Λ) of the PCF is around 0.414. Figures 1(c) and 1(d) show the electric field profile of the core mode (LP_{01}) and one of the higher order cladding modes (LP_{11}) of the PCF. These are generated using the finite element method (FEM) from COMSOL Multiphysics (version 4.4).

Because the SMF and the PCF have the same diameter, the splicing becomes easier with a commercial splicing machine. The splicing leads to the collapse of the PCF voids over a distance of 200 μm at the joint of the SMF and PCF [20]. After splicing one end of the PCF with the SMF, the other end is cleaved with a standard cleaving machine (Sumitomo electric) so that it acts as a mirror because of Fresnel reflection. When light from the broadband source is coupled to the SMF via the circulator, the fundamental mode of the SMF diffracts at the splicing joint. This leads to the broadening of the modes which, in turn, excites the core and cladding modes in the PCF [21–24]. These modes propagate up to the cleaved end of the PCF from where they are reflected back. The reflected modes again coupled to the PCF where they recombined with the SMF core mode. The difference in the propagation constants of core and cladding mode results in phase difference between them. This accumulated phase difference depends on the distance traveled and the wavelength of operation. Thus, depending on the phase difference and wavelength, a series of maxima and minima are obtained in the reflection spectrum as shown in Fig. 2. However, adding an external mirror creates another cavity between the tip of the PCF and the mirror giving rise to a composed interference pattern as shown in Fig. 2. It can be noted that the external cavity discretizes the interference pattern of the mode interferometer. This helps to monitor displacements with nanometric resolution as the position of narrow fringes can be tracked with higher precision.

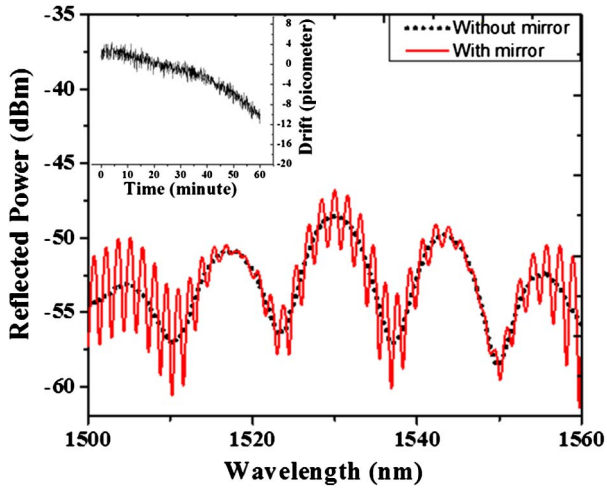

Fig. 2. Interference pattern obtained because of two different cases. The black dotted line refers to the interference pattern without the mirror, and the red line refers to that with the mirror. The length of the PCF considered is 26 mm. The inset shows the drift of the interference pattern with time.

The interference pattern in presence and in absence of an external mirror can be described by Eqs. (1) and (2), respectively, as shown below [25].

$$I_{\text{without mirror}}(\lambda) = \left|\left(\frac{E_1 + E_2}{E_0}\right)\right|^2, \tag{1}$$

$$I_{\text{mirror}}(\lambda) = \left|\left(\frac{E_1 + E_2 + E_3 + E_4}{E_0}\right)\right|^2, \tag{2}$$

where

$$E_1 = \alpha\sqrt{R_1}E_0 e^{-j2\phi_1}, \qquad E_2 = (1-\alpha)\sqrt{R_2}E_0 e^{-j2\phi_2},$$
$$E_3 = \alpha\sqrt{R_3}(1-R_1)E_0 e^{-j(2\phi_1+2\phi_3)},$$
$$E_4 = (1-\alpha)\sqrt{R_3}(1-R_2)E_0 e^{-j(2\phi_2+2\phi_3)}.$$

The symbol I refers to the interference pattern, E_1 and E_2 refer to the total reflected electric field of the core, and clad mode from the tip of PCF and E_3 and E_4 refer to electric fields from mirror and E_0 to the input electric field. The symbol α refers to the fraction of light in cladding; R_1, R_2, and R_3 are reflection coefficients at the PCF end surface for core and cladding and gold mirror, respectively; and ϕ_1, ϕ_2, and ϕ_3 are round trip propagation phase shifts introduced because of the core, cladding, and the external mirror, respectively. The extra cavity helps in the formation of the narrow fringe pattern, and the term ϕ_3 is responsible for the shifting of these patterns as it is a function of the distance between the tip of the PCF and the mirror.

One of the important performance parameters of the interferometric sensors is the stability of the interference pattern, since for sensing applications one measures the shift of the latter. The high stability with time is expected as in our interferometer a single splice carries out the splitting and recombination of modes. Moreover, the

splice is permanent and does not degrade with time or with temperature. To determine the stability of the interference pattern with time, we used a fiber Bragg grating interrogator from Ibsen Photonics. The drift over a time period of one hour observed in the interference pattern of an interferometer built with 13 mm of the aforementioned PCF is shown in the inset of Fig 2. As can be seen from the figure, the total drift in the interference pattern is 16 pm over a period of an hour. The stability of our proposed device is comparable with that reported in [21]. As for our measurements, the complete tracking of the interference pattern with displacement takes less than one minute; thus the drift of a particular interference pattern with time is much less (<1 pm) and hence insignificant. This is negligible in comparison to the shift in the interference pattern because of the displacement of the mirror that has been used for the nano-displacement sensor. The experiment is performed at room temperature. The sensitivity of the sensor at room temperature is negligible and hence does not affect the performance significantly.

To make sure that the light reflected from the external mirror coupled back to the sensor head effectively, we monitored the reflected power with a suitable photodetector. The mirror is adjusted in such a way that the power meter shows maximum intensity. Here, the mirror is kept at distances ranging from 110 to 720 μm from the tip of the sensing head. We found that, for relatively larger distance away from the tip of the PCF, the interference pattern resulting from the external mirror disappears as the reflected light from the mirror is lost because of the divergence of the reflected beam, and hence the light that couples to the PCF reduces. Moreover, keeping the mirror too close to the tip of the PCF leads to the reduction in the degrees of freedom of movement.

The narrow fringes of the composed interference pattern produced because of the setup are very sensitive to the change in position of the mirror. The response of the device to the displacement (d) is analyzed by moving the mirror with the help of a nanopositioner. The mirror mounted on the nanopositioner is controlled by a controller operating in a closed loop. The response of the fabricated sensor is observed by displacing the mirror from $d = 0$ nm to $d = 100$ nm at an interval of 10 nm. The mirror is kept at several positions away from the tip of the PCF. Then for each position, the mirror is displaced by a step of 10 nm toward the tip of the PCF. The variation of the peak position with displacement is found to be linear as seen in Fig. 3. It can be noted that, for a displacement of 100 nm, the peak shifts 3.2 nm. The inset (top corner) in Fig. 3 shows the interference pattern corresponding to $d = 110$ μm. As we keep the mirror closer to the facet of the PCF, the pattern gets distorted as shown in the inset (bottom corner) of Fig. 3 for $d = 80$ μm.

When the mirror is kept closer to the PCF, the cavity length gets reduced which leads to an increase in the period of the interference pattern. Thus, the period of the PCF interferometer may coincide with that of the Fabry–Perot cavity. On the other hand, for larger values of d, the coupling of the reflected light to the PCF decreases because of the diffraction loss. Thus we kept the mirror at several positions ranging from 110 to

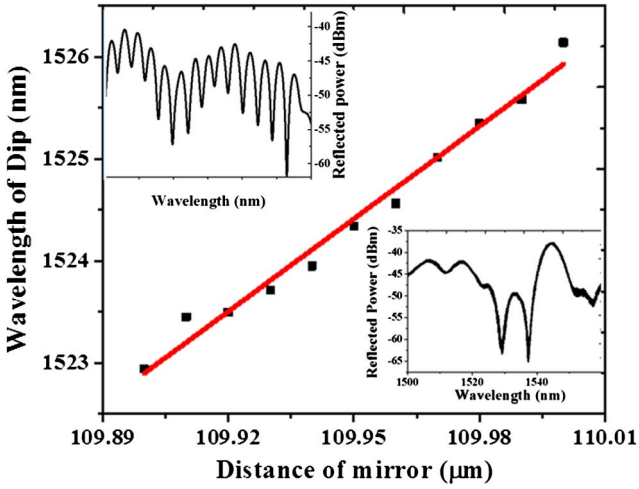

Fig. 3. Change in wavelength of dip corresponding to 1526.14 nm with distance of mirror. The inset figures show the interference pattern for position of the mirror with $d = 110$ μm (top corner) and $d = 80$ μm (bottom corner), respectively.

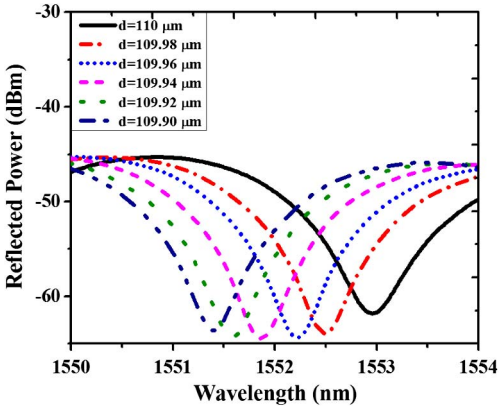

Fig. 4. Shift of interference pattern with distance between the mirror and the tip of PCF.

700 μm. When the mirror distance is kept at 110 μm and the mirror is displaced gradually, the wavelength corresponding to the dip shifts toward the lower wavelength as can be seen in Fig. 4.

To calculate the displacement sensitivity which is defined as a shift in the dip of the interference pattern per unit change in displacement of the mirror, we plotted the shift in the interference pattern with the displacement of the mirror for three values of d. As seen in Fig. 5, the peak shift is linear for all three values of d. The maximum sensitivity of 32 pm/nm is obtained for a cavity length of 110 μm as seen in Fig. 6. At a higher value of cavity length, the sensitivity decreases.

The minimum detectable displacement for this sensor depends on the resolution of the detector. In our case, the displacement sensitivity is 32 pm/nm and the OSA has a resolution of 10 pm. Considering this, the minimum detectable displacement of our sensor is 0.31 nm. Although this resolution is less than compared to laser heterodyne interferometer, one can achieve a better resolution using a detector having a resolution less than 10 pm with our compact setup. The variation of sensitiv-

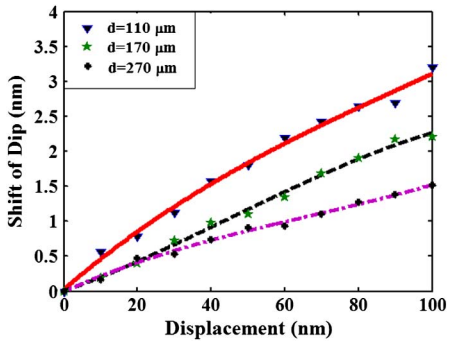

Fig. 5. Variation of sensitivity with displacement of mirror for different d values. The symbols and continuous lines show the experimental data and fitted curve, respectively.

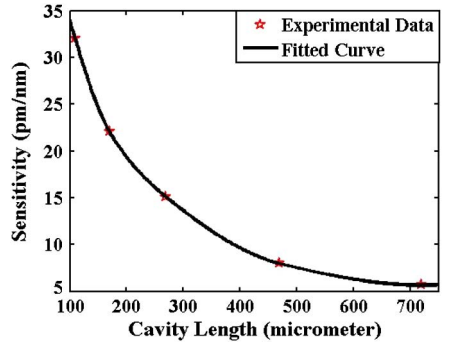

Fig. 6. Variation of sensitivity with cavity length.

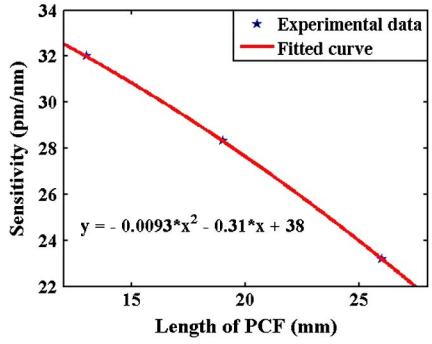

Fig. 7. Variation of sensitivity with length of the PCF. The fitted curve equation is shown in the inset.

ity with length of the PCF has also been investigated. As seen in Fig. 7, the sensitivity is the maximum for a PCF with a length of 13 mm. Thus the sensor can be used for the detection of nano-displacement over a range of 100–700 μm, i.e., the sensor has broad dynamic range, and can be suitable for a range of applications that involve precision alignment or positioning.

In summary, a compact reflection based modal interferometer consisting of a SMF and a small piece of PCF for nano-displacement measurement is proposed. The use of a highly reflecting target forms an extra cavity and the resulting interference pattern resulting from the coupling of reflected light from the tip of the PCF and the external mirror is found to be very sensitive to the displacement of the mirror. The displacement sensitivity of the sensor is found to be 32 pm/nm. The sensor can be used in structural health monitoring and for the detection of nonuniformity on electronic chips in nanoscale. So the proposed setup can be used for accurate measurement of the displacements in nanoscale which will be very useful in the field of industrial and scientific research.

References

1. F. Taffoni, D. Formica, P. Saccomandi, G. D. Pino, and E. Schena, Sensors **13**, 14105 (2013).
2. L. H. Kang, D. K. Kim, and J. H. Han, J. Sound Vib. **305**, 534 (2007).
3. J. Manwell, G. Bailey, P. Parsons, P. Richards, and D. Kreit, Sens. Actuators **18**, 233 (1989).
4. S. Fourment, P. Arguel, J. L. Noullet, F. Lozes, S. Bonnefont, G. Sarrabayrouse, Y. Jourlin, J. Jay, and O. Parriaux, Sens. Actuators A **110**, 294 (2004).
5. X. Li and G. C. M. Meijer, IEEE Trans. Instrum. Meas. **44**, 3 (1995).
6. X. Li, C. Yang, S. Yang, and G. Li, Sensors **12**, 12544 (2012).
7. D. T. Smith, J. R. Pratt, and L. P. Howard, Rev. Sci. Instrum. **80**, 035105 (2009).
8. L. M. Manojlovic, Opt. Lasers Eng. **48**, 486 (2010).
9. X. Y. Dong, X. Yang, C.-L. Zhao, L. Ding, P. Shum, and N. Q. Ngo, Smart Mater. Struct. **14**, N7 (2005).
10. J. M. Baptista, S. F. Santos, G. Rego, O. Frazao, and J. L. Santos, Opt. Commun. **260**, 8 (2006).
11. C. J. Lin and F. G. Tseng, Sens. Actuators, A **114**, 163 (2004).
12. T. Yokoyama, T. Araki, S. Yokoyama, and N. Suzuki, Meas. Sci. Technol. **12**, 157 (2001).
13. E. Zhang, Q. Hao, B. Chen, L. Yan, and Y. Liu, Opt. Express **22**, 25587 (2014).
14. C. Fan, C. Chiang, and C. Yu, Opt. Express **19**, 19948 (2011).
15. B. Dong and E. J. Hao, J. Opt. Soc. Am. B **28**, 2332 (2011).
16. M. Bravo, A. M. R. Pinto, M. Lopez-Amo, J. Kobelke, and K. Schuster, Opt. Lett. **37**, 202 (2012).
17. A. Margarida, R. Pinto, J. M. Baptista, J. L. Santos, M. Lopez-Amo, and O. Frazao, Sensors **12**, 17497 (2012).
18. O. Levy, B. Z. Steinberg, M. Nathan, and A. Boag, Appl. Phys Lett. **86**, 104102 (2005).
19. P. S. J. Russell, IEEE J. Lightwave Technol. **24**, 4729 (2006).
20. R. Jha, J. Villatoro, G. Badenes, and V. Pruneri, Opt. Lett. **34**, 617 (2009).
21. R. Jha, J. Villatoro, and G. Badenes, Appl. Phys. Lett. **93**, 191106 (2008).
22. M. Deng, X. Sun, H. Wei, and J. Li, IEEE Photon. Technol. Lett. **26**, 531 (2014).
23. W. Qian, C. L. Zhao, C. C. Chan, L. Hu, T. Li, W. C. Wong, P. Zu, and X. Dong, IEEE Sensors J. **12**, 2593 (2012).
24. S. Qiu, Y. Chen, F. Xu, and Y. Lu, Opt. Lett. **37**, 863 (2012).
25. Y. J. Rao, M. Deng, D. W. Duan, and T. Zhu, Sens. Actuators A **148**, 33 (2008).